An orbital invariant similarity constrained coupled cluster model

Eirik F. Kjønstad[†,‡] and Henrik Koch[*,‡,†]

[†]*Department of Chemistry, Norwegian University of Science and Technology, 7491 Trondheim, Norway*

[‡]*Scuola normale superiore, Piazza dei Cavalieri, 7, 56126 Pisa PI, Italy*

E-mail: henrik.koch@ntnu.no

Abstract

We present a similarity constrained coupled cluster method able to describe conical intersections between two excited electronic states of the same symmetry. For a given pair of states, this singles and doubles method (SCCSD) is unique and orbital invariant. The computational cost scales as the sixth power with respect to the number of orbitals, and preliminary calculations indicate that the excitation energy difference relative to CCSD is within the error range of CCSD (approximately 0.10 eV). We also analyze the size-scaling properties of the orthogonality condition. For a projected orthogonality condition we show, and demonstrate numerically, that the method is rigorously size-intensive.

1 Introduction

The importance of nonadiabatic phenomena in excited state chemistry—resulting from the prevalence of electronic degeneracies, or conical intersections—is widely recognized.[1] While

ground state chemistry is often treated succesfully by adiabatic dynamics within the Born-Oppenheimer[2] approximation, the fate of excited electronic states following photoexcitation typically involve many potential energy surfaces. To describe such processes theoretically, the applied electronic structure method must describe excited states with high accuracy, and the nuclei must be treated quantum mechanically or semi-classically.[3,4] The interest in nonadiabatic simulation methods has increased in recent decades, but the field has a long history. Established methods include, but are not limited to, surface hopping,[5,6] multiple spawning,[4,7,8] mean-field Ehrenfest dynamics,[9] and multiconfiguration time-dependent Hartree.[10]

Regardless of the nuclear dynamics method, a sufficiently accurate treatment of the electronic wavefunctions is necessary to obtain reliable predictions. For instance, a balanced description of dynamical and nondynamical electron correlation is crucial when nuclei pass through a conical intersection.[3] Given their high accuracy, it would be useful, in certain cases, to treat the electronic structure using the linear response[11] or equation of motion[12] coupled cluster methods. As long as the ground state is dominated by a single determinant, coupled cluster theory accurately accounts for dynamical correlation, but it can also describe multireference character in the excited electronic states due to the linear parametrization of these states.[13] Close to conical intersections, the electronic states attain multireference character. Consequently, near-degeneracies between excited states are in general treatable, whereas near-degeneracies with the ground state are not.

The electronic structure quantities needed for coupled cluster dynamics simulations have been studied extensively. The calculation of analytical gradients is well-established in coupled cluster theory,[14,15] and implementations and derivations of nonadiabatic coupling vectors have been reported,[16–19] most recently the equation of motion singles and doubles (EOM-CCSD)[12,20] implementation by Faraji *et al.*[19] Evidently, much of the machinery needed to perform coupled cluster dynamics is already available, yet using the method for excited state dynamics is difficult given its well-known problems at conical intersections between

electronic states of the same symmetry.[21–23] The existence of such problematic regions was first postulated and characterized by Hättig,[21] who observed that complex energy pairs were to be expected due to the non-Hermiticity of coupled cluster theory. Hättig also argued that the dimensionality of the intersections would be incorrect, rendering the surfaces qualitatively incorrect close to electronic degeneracies.[21] In this context, coupled cluster methods are called non-Hermitian because the excitation energies are eigenvalues of a non-Hermitian matrix $\boldsymbol{\mathcal{A}}$ known as the Jacobian.[11,12] The existence of complex energies was first confirmed numerically by Köhn and Tajti[22] in calculations using coupled cluster singles and doubles (CCSD) and triples (CCSDT)[24,25] theory. More recently, complex energies have also been reported in a surface hopping simulation on adenine using the perturbative doubles (CC2)[26] model.[27]

As shown by von Neumann and Wigner,[28] and by Teller,[29] a conical intersection between two electronic states, for real Hamiltonians, can exist in an $N-2$ dimensional subspace of the internal nuclear coordinate space, where N is the number of internal coordinates. Two conditions must be satisfied at an intersection. Expressed in the subspace of the two eigenstates, the diagonal elements of the electronic Hamiltonian H have to be equal ($H_{11} = H_{22}$) and the off-diagonal element has to vanish ($H_{12} = 0$).[29] In coupled cluster theory, the analysis is more involved. If $\boldsymbol{\mathcal{A}}$ is assumed to be diagonalizable, three conditions are satisfied at an intersection due to the non-symmetry of $\boldsymbol{\mathcal{A}}$:

$$\mathcal{A}_{11} = \mathcal{A}_{22}, \quad \mathcal{A}_{12} = 0, \quad \mathcal{A}_{21} = 0. \tag{1}$$

If diagonalizability is not assumed, only one condition is obtained:

$$(\mathcal{A}_{22} - \mathcal{A}_{11})^2 + 4\mathcal{A}_{12}\mathcal{A}_{21} = 0. \tag{2}$$

Both cases appear to give the wrong number of conditions.[21,23]

We say that $\boldsymbol{\mathcal{A}} = \boldsymbol{\mathcal{A}}(\boldsymbol{R})$ is non-diagonalizable/defective at the molecular geometry $\boldsymbol{R}$ if the algebraic multiplicity of an eigenvalue of $\boldsymbol{\mathcal{A}}$ exceeds its geometric multiplicity.[30,31] At a

two-state intersection, $\boldsymbol{\mathcal{A}}$ can, for instance, have a doubly degenerate eigenvalue associated with one eigenvector. Upon approaching this geometry, the two eigenvectors gradually collapse and become parallel, reducing the number of eigenvectors by one. The term 'defective' is used to emphasize that non-diagonalizable points are unphysical for Hamiltonian matrices where the eigenvectors represent the electronic states.[23]

Recently, we reconsidered the question of intersection dimensionality and the causes of the nonphysical behavior in coupled cluster theory.[23,32] First we noted that since diagonalizability cannot be assumed at same-symmetry intersections, the intersection seam, defined as the space where there is an eigenvalue degeneracy,[1] has the dimensionality $N-1$. The numerical evidence confirms this,[22,23] seemingly supporting the claim that the intersection is qualitatively incorrect. However, the seam has some interesting geometrical features. By mapping out two potential energy surfaces in hypofluorous acid, for which $N=3$, we found that the seam is folded. It is cylindrically shaped with complex energies in its interior and a defective, degenerate eigenvalue on its two-dimensional surface ($N-1=2$). The geometry of the seam can be understood from the exact limit of the theory. Because the coupled cluster hierarchy converges to the full configuration-interaction (CI) limit, the cylinder-shaped intersection seam must shrink to become a curve as more excitations enter the cluster operator, gradually altering its dimensionality from $N-1$ to the correct $N-2$.[23]

A nondefective $\boldsymbol{\mathcal{A}}$ implies that the three conditions in Eq. (1) are satisfied at a conical intersection. This does not mean that the dimensionality of the seam is $N-3$, however. As long as $\boldsymbol{\mathcal{A}}(\boldsymbol{R})$ is nondefective for all $\boldsymbol{R}$, the three conditions are redundant.[23] For example, the untruncated limit gives the correct $N-2$ dimensionality even though $\boldsymbol{\mathcal{A}}$ is non-Hermitian in this limit. More generally, this means that making $\boldsymbol{\mathcal{A}}$ nondefective represents an approach to obtain correctly shaped conical intersections with seams of the correct dimensionality.[23,32] Another approach is to employ non-standard Hermitian coupled cluster models, such as the unitary and variational approaches investigated by some researchers in the field.[33–36]

Defects are avoided in the full CI limit because the eigenvectors of $\boldsymbol{\mathcal{A}}$ become, in that limit,

orthogonal with respect to a positive definite matrix $\boldsymbol{\mathcal{M}}$. This ensures that two eigenstates never become parallel, eliminating the possibility of a defective eigenvalue in their subspace.[23] A useful corrolary is that intersections between two states are described correctly as long as the eigenvectors are $\boldsymbol{\mathcal{M}}$-orthogonal. In the similarity constrained coupled cluster (SCC)[32] method recently introduced by us, $\boldsymbol{\mathcal{M}}$-orthogonality is enforced among two or more states using a similarity transformation of the electronic Hamiltonian—in particular, a similarity transformation of the standard similarity transformed Hamiltonian in coupled cluster theory. By using a simple similarity constrained model, SCCSD, in which a single triple-excitation is added to the CCSD cluster operator, we were able to show that an intersection seam in hypofluorous acid became $N-2$ dimensional. The potential energy surfaces also exhibited the proper conical shape in the branching plane of an intersection point.[32]

In this work we present a more robust similarity constrained model to address the two main limitations we identified in the single-excitation model, the lack of orbital invariance and the non-trivial selection of triple excitation.[32] To obtain orbital invariance, we use a triple excitation operator that consists of the single and double excited state operators of the right eigenstates. This also preserves the size-extensive and size-intensive structure of the ground and excited state equations. Furthermore, we show that one may apply a projection operator in $\boldsymbol{\mathcal{M}}$ to obtain a size-intensive orthogonality condition. As a result, the model satisfies all the proper size-scaling criteria, meaning that no inconsistency errors are introduced in the ground or excited state energies or wavefunctions. The computational cost of the model is still $O(M^6)$, where M is the number of orbitals, and the only input the user needs to specify are the states that are to be made $\boldsymbol{\mathcal{M}}$-orthogonal.

2 The similarity constrained coupled cluster model

2.1 Theory

We define the ground state wavefunction as

$$|\mathrm{CC}\rangle = e^{\mathcal{T}}|\mathrm{HF}\rangle, \quad \mathcal{T} = T + X_3 = T_1 + T_2 + X_3, \tag{3}$$

where $|\mathrm{HF}\rangle$ is the closed-shell Hartree-Fock state. The single and double excitation contributions to $\mathcal{T}$ are

$$T_1 = \sum_{ai} t_i^a E_{ai}, \quad T_2 = \frac{1}{2}\sum_{aibj} t_{ij}^{ab} E_{ai} E_{bj}, \tag{4}$$

where $i, j, \ldots$ and $a, b, \ldots$ denote occupied and virtual orbitals and $E_{ai} = a_{a\alpha}^\dagger a_{i\alpha} + a_{a\beta}^\dagger a_{i\beta}$. In this work we restrict ourselves to singlet states, though we note that a generalization to triplet states is straightforward.[37,38] The triple excitation operator in $\mathcal{T}$ is expressed as

$$X_3 = \frac{1}{6}\sum_{aibjck} x_{ijk}^{abc} E_{ai} E_{bj} E_{ck}, \tag{5}$$

and the similarity transformed Hamiltonian as

$$\bar{\mathcal{H}} = e^{-\mathcal{T}} H e^{\mathcal{T}} = e^{-X_3}(e^{-T} H e^{T}) e^{X_3} = e^{-X_3} \bar{H} e^{X_3}, \tag{6}$$

where $\bar{H} = e^{-T} H e^{T}$ is known as the standard similarity transformed Hamiltonian.[39] The purpose of X_3 is to constrain $\bar{\mathcal{H}}$ so that two excited electronic states become $\boldsymbol{\mathcal{M}}$-orthogonal.

In the reference, single and double excitation space, the governing equations are identical to the standard coupled cluster equations, except that corrections due to X_3 are accounted

for. We compute the ground state energy using the standard expression

$$E_0 = \langle \mathrm{HF} | \bar{\mathcal{H}} | \mathrm{HF} \rangle = \langle \mathrm{HF} | \bar{H} | \mathrm{HF} \rangle, \tag{7}$$

and solve the amplitude equations

$$\Omega_\mu = \langle \mu | \bar{\mathcal{H}} | \mathrm{HF} \rangle = \langle \mu | e^{-X_3} \bar{H} e^{X_3} | \mathrm{HF} \rangle = 0 \tag{8}$$

for singly and doubly excited kets $|\mu\rangle = \tau_\mu |\mathrm{HF}\rangle$. Here $\{\tau_\mu\}$ is the set $\{E_{ai}, E_{ai}E_{bj}\}$ of spin-free excitation operators. For the corresponding bra vectors $\langle\mu|$, we use linear combinations of these excitation operators in order to ensure biorthonormality with the kets $|\mu\rangle$.

The electronic states are, as in equation of motion coupled cluster theory, represented by $\{\boldsymbol{\mathcal{L}}_0, \boldsymbol{\mathcal{L}}_1, \boldsymbol{\mathcal{L}}_2, \ldots\}$ and $\{\boldsymbol{\mathcal{R}}_0, \boldsymbol{\mathcal{R}}_1, \boldsymbol{\mathcal{R}}_2, \ldots\}$, the left and right eigenvectors of the Jacobian $\boldsymbol{\mathcal{A}}$, respectively. The $\boldsymbol{\mathcal{A}}$ matrix may be defined as

$$\begin{aligned} \mathcal{A}_{\mu\nu} &= \langle \mu | (\bar{\mathcal{H}} - E_0) | \nu \rangle \\ &= \langle \mu | e^{-X_3} (\bar{H} - E_0) e^{X_3} | \nu \rangle, \quad \mu, \nu \geq 0, \end{aligned} \tag{9}$$

where we let $|0\rangle \equiv |\mathrm{HF}\rangle$ and otherwise restrict μ and ν to single and double excitations with respect to $|\mathrm{HF}\rangle$. The left eigenvectors represent the bra states, and the right eigenvectors the ket states, in expectation values and transition matrix elements between electronic states. The eigenvalues of $\boldsymbol{\mathcal{A}}$ are the excitation energies, $\omega_n = E_n - E_0$.[11,12]

For convenience, the ground and excited states of $\boldsymbol{\mathcal{A}}$ are usually treated separately. By defining $\boldsymbol{\eta}$ and $\boldsymbol{A}$ as

$$\eta_\nu = \langle \mathrm{HF} | \bar{\mathcal{H}} | \nu \rangle \tag{10}$$

$$A_{\mu\nu} = \langle \mu | \bar{\mathcal{H}} | \nu \rangle - \delta_{\mu\nu} E_0, \tag{11}$$

where $\mu, \nu > 0$, we can partition $\boldsymbol{\mathcal{A}}$ according to $|\mathrm{HF}\rangle$ and $\{|\mu\rangle : \mu > 0\}$ contributions.

Assuming that $\boldsymbol{\Omega} = \mathbf{0}$, we have

$$\boldsymbol{\mathcal{A}} = \begin{pmatrix} 0 & \boldsymbol{\eta}^T \\ \mathbf{0} & \boldsymbol{A} \end{pmatrix}. \tag{12}$$

This block structure implies that the left and right ground states are

$$\boldsymbol{\mathcal{L}}_0 = \begin{pmatrix} 1 \\ \bar{\boldsymbol{t}} \end{pmatrix}, \quad \boldsymbol{\mathcal{R}}_0 = \begin{pmatrix} 1 \\ \mathbf{0} \end{pmatrix} \tag{13}$$

provided the multiplier vector[40] $\bar{\boldsymbol{t}}$ satisfies

$$\boldsymbol{\eta}^T + \bar{\boldsymbol{t}}^T \boldsymbol{A} = \mathbf{0}. \tag{14}$$

The left ground state $\boldsymbol{\mathcal{L}}_0$ is often referred to as the "lambda" state (and denoted $\langle\Lambda|$) when expressed in the left basis $\{\langle \mathrm{HF}|e^{-\mathcal{T}}, \langle\mu|e^{-\mathcal{T}}\}$. Analogously, $\boldsymbol{\mathcal{R}}_0$ is the coupled cluster state $|\mathrm{CC}\rangle$ when expressed in the right basis $\{e^{\mathcal{T}}|\mathrm{HF}\rangle, e^{\mathcal{T}}|\mu\rangle\}$.[11,39] Making use of the biorthogonality of the left and right eigenvectors, we can express the excited states ($n = 1, 2, \ldots$) as

$$\boldsymbol{\mathcal{L}}_n = \begin{pmatrix} 0 \\ \boldsymbol{L}_n \end{pmatrix}, \quad \boldsymbol{\mathcal{R}}_n = \begin{pmatrix} -\bar{\boldsymbol{t}}^T \boldsymbol{R}_n \\ \boldsymbol{R}_n \end{pmatrix} \equiv \begin{pmatrix} R_n^0 \\ \boldsymbol{R}_n \end{pmatrix} \tag{15}$$

The $\{|\mu\rangle : \mu > 0\}$ state-contributions satisfy the eigenvalue equations

$$\boldsymbol{A}\boldsymbol{R}_n = \omega_n \boldsymbol{R}_n \tag{16}$$

$$\boldsymbol{L}_n^T \boldsymbol{A} = \omega_n \boldsymbol{L}_n^T, \quad n = 1, 2, \ldots \tag{17}$$

Note that it is $\boldsymbol{A}$ that is usually called the Jacobian in the literature,[11,39] although we use the same term when referring to the extended matrix $\boldsymbol{\mathcal{A}}$.[23,32]

We have already noted that the right eigenvectors of $\boldsymbol{\mathcal{A}}$ are orthogonal with respect to a positive definite metric $\boldsymbol{\mathcal{M}}$ when the excitation space is untruncated. The proof is as follows.

Suppose that $\{|\mu\rangle : \mu \geq 0\}$ is an orthonormal basis. Then $I = \sum_{\mu\geq 0} |\mu\rangle\langle\mu|$ and so

$$\begin{aligned}(\boldsymbol{\mathcal{A}} + E_0\boldsymbol{I})_{\mu\nu} &= \langle\mu\,|\,e^{-\mathcal{T}} H e^{\mathcal{T}}\,|\,\nu\rangle \\ &= \sum_{\sigma\tau\geq 0} \langle\mu\,|\,e^{-\mathcal{T}}\,|\,\sigma\rangle\langle\sigma\,|\,H\,|\,\tau\rangle\langle\tau\,|\,e^{\mathcal{T}}\,|\,\nu\rangle \\ &= (\boldsymbol{\mathcal{Q}}^{-1}\boldsymbol{\mathcal{H}}\,\boldsymbol{\mathcal{Q}})_{\mu\nu},\end{aligned} \tag{18}$$

where $\mathcal{Q}_{\mu\nu} = \langle\mu\,|\,e^{\mathcal{T}}\,|\,\nu\rangle$ transforms the eigenvectors of $\boldsymbol{\mathcal{A}}$ to those of $\boldsymbol{\mathcal{H}}$. Orthonormality of the eigenvectors of $\boldsymbol{\mathcal{H}}$ implies that the eigenvectors of $\boldsymbol{\mathcal{A}}$ are orthonormal with respect to the positive-definite matrix $\boldsymbol{\mathcal{M}} \equiv \boldsymbol{\mathcal{Q}}^T\boldsymbol{\mathcal{Q}}$. In other words,

$$\begin{aligned}\mathcal{O}_{kl}(\boldsymbol{\mathcal{M}}) &\equiv \boldsymbol{\mathcal{R}}_k^T\boldsymbol{\mathcal{M}}\,\boldsymbol{\mathcal{R}}_l \\ &= \boldsymbol{\mathcal{R}}_k^T\boldsymbol{\mathcal{Q}}^T\boldsymbol{\mathcal{Q}}\,\boldsymbol{\mathcal{R}}_l \\ &= \delta_{kl}, \quad k,l = 0,1,2,\ldots.\end{aligned} \tag{19}$$

For same-symmetry states, these $\boldsymbol{\mathcal{M}}$-orthogonality relations cease to hold for truncated excitation spaces and must in that case be enforced.[23] This is possible not only for orthogonalities between excited states, but also between the ground and first excited state. However, as noted, ground state intersections can only be described using a model that is able to treat multireference character in the ground state.

In the original similarity constrained model, we truncated μ and ν in $\mathcal{Q}_{\mu\nu}$ to include the reference as well as single and double excitations. Then we imposed $\mathcal{O}_{ab}(\boldsymbol{\mathcal{M}}) = 0$ for a pair of states $\{\boldsymbol{\mathcal{R}}_a, \boldsymbol{\mathcal{R}}_b\}$.[32] In this work, we introduce the projected orthogonality relation

$$\begin{aligned}\mathcal{O}_{ab}(\boldsymbol{\mathcal{M}}_{\boldsymbol{\mathcal{P}}}) &= \boldsymbol{\mathcal{R}}_a^T\boldsymbol{\mathcal{M}}_{\boldsymbol{\mathcal{P}}}\,\boldsymbol{\mathcal{R}}_b \\ &\equiv \boldsymbol{\mathcal{R}}_a^T\boldsymbol{\mathcal{Q}}^T\boldsymbol{\mathcal{P}}\boldsymbol{\mathcal{Q}}\,\boldsymbol{\mathcal{R}}_b = 0\end{aligned} \tag{20}$$

where $\boldsymbol{\mathcal{P}}$ is the projection operator onto the subspace spanned by $\{\boldsymbol{\mathcal{R}}_a, \boldsymbol{\mathcal{R}}_b\}$.

Before discussing the size-scaling properties of Eqs. (19) and (20), let us express the or-

thogonality conditions in a form more convenient for implementation purposes. Partitioning $\boldsymbol{\mathcal{Q}}$ into $|\mathrm{HF}\rangle$ and $\{|\mu\rangle : \mu > 0\}$ contributions, we get

$$\boldsymbol{\mathcal{Q}} = \begin{pmatrix} 1 & \mathbf{0} \\ \boldsymbol{q} & \boldsymbol{Q} \end{pmatrix}. \tag{21}$$

Then, writing

$$\boldsymbol{\mathcal{R}}_k = \begin{pmatrix} R_k^0 \\ \boldsymbol{R}_k \end{pmatrix} \tag{22}$$

we find that

$$\boldsymbol{\mathcal{C}}_k \equiv \boldsymbol{\mathcal{Q}}\boldsymbol{\mathcal{R}}_k = \begin{pmatrix} R_0^k \\ R_0^k \boldsymbol{q} + \boldsymbol{Q}\boldsymbol{R}_k \end{pmatrix}. \tag{23}$$

The non-projected overlap can hence be written as

$$\begin{aligned} \mathcal{O}_{kl}(\boldsymbol{\mathcal{M}}) =& R_k^0 R_l^0 (1 + \boldsymbol{q}^T \boldsymbol{q}) + R_k^0 \boldsymbol{q}^T \boldsymbol{Q} \boldsymbol{R}_l \\ &+ \boldsymbol{R}_k^T \boldsymbol{Q}^T \boldsymbol{q} R_l^0 + \boldsymbol{R}_k^T \boldsymbol{Q}^T \boldsymbol{Q} \boldsymbol{R}_l. \end{aligned} \tag{24}$$

The projected overlap is conveniently expressed as

$$\begin{aligned} \mathcal{O}_{kl}(\boldsymbol{\mathcal{M}}_{\boldsymbol{\mathcal{P}}}) &= (\boldsymbol{W}^T \boldsymbol{G}^{-1} \boldsymbol{W})_{kl} \\ &= \sum_{m,n=a,b} W_{km}^T G_{mn}^{-1} W_{nl}, \end{aligned} \tag{25}$$

where it is understood that $k, l = a, b$, and where

$$G_{kl} = \boldsymbol{\mathcal{R}}_k^T \boldsymbol{\mathcal{R}}_l \tag{26}$$

$$W_{kl} = \boldsymbol{\mathcal{R}}_k^T \boldsymbol{\mathcal{Q}} \boldsymbol{\mathcal{R}}_l. \tag{27}$$

The expression in Eq. (25) follows from inserting

$$\boldsymbol{\mathcal{P}} = \sum_{m,n=a,b} \boldsymbol{\mathcal{R}}_m G^{-1}_{mn} \boldsymbol{\mathcal{R}}^T_n \tag{28}$$

into Eq. (20). To compute the elements of $\boldsymbol{G}$ and $\boldsymbol{W}$, we partition into $|\mathrm{HF}\rangle$ and $\{|\mu\rangle : \mu > 0\}$ contributions, rewriting Eqs. (26) and (27) as

$$G_{kl} = R^k_0 R^l_0 + \boldsymbol{R}^T_k \boldsymbol{R}_l \tag{29}$$

$$W_{kl} = R^k_0 R^l_0 + \boldsymbol{R}^T_k (R^l_0 \boldsymbol{q} + \boldsymbol{Q}\boldsymbol{R}_l). \tag{30}$$

Programmable expressions are given in Section 2.2.

We introduce $\mathcal{O}_{ab}(\boldsymbol{\mathcal{M}}_{\boldsymbol{\mathcal{P}}})$ because it satisfies size-intensivity. For the non-projected overlap $\mathcal{O}_{ab}(\boldsymbol{\mathcal{M}})$, size-intensivity is satisfied only when the excitation space is not truncated. To see why the overlap should be size-intensive, consider two non-interacting subsystems C and D. Let $\boldsymbol{\mathcal{R}}^{\mathrm{C}}_a$ and $\boldsymbol{\mathcal{R}}^{\mathrm{C}}_b$ be states located on system C with block structure denoted as

$$\boldsymbol{\mathcal{R}}^{\mathrm{C}}_a = \begin{pmatrix} R^0_a \\ \boldsymbol{R}_a \end{pmatrix}, \quad \boldsymbol{\mathcal{R}}^{\mathrm{C}}_b = \begin{pmatrix} R^0_b \\ \boldsymbol{R}_b \end{pmatrix}. \tag{31}$$

Excited states are size-intensive in the sense that an excited state on C is also an excited state of the non-interacting CD system. Let us order the CD excitation manifold as

$$\{|\mathrm{HF_C}\rangle|\mathrm{HF_D}\rangle, |\mu_{\mathrm{C}}\rangle|\mathrm{HF_D}\rangle, |\mathrm{HF_C}\rangle|\mu_{\mathrm{D}}\rangle, |\mu_{\mathrm{CD}}\rangle\}. \tag{32}$$

Then the states

$$\boldsymbol{\mathcal{R}}^{\mathrm{CD}}_a = \begin{pmatrix} R^0_a \\ \boldsymbol{R}_a \\ \boldsymbol{0} \\ \boldsymbol{0} \end{pmatrix}, \quad \boldsymbol{\mathcal{R}}^{\mathrm{CD}}_b = \begin{pmatrix} R^0_b \\ \boldsymbol{R}_b \\ \boldsymbol{0} \\ \boldsymbol{0} \end{pmatrix}, \tag{33}$$

can be shown to satisfy the CD equations with the same excitation energies as the isolated C system.[41] Consequently, if the overlap is zero in system C (for $\boldsymbol{\mathcal{R}}_a^{\mathrm{C}}$ and $\boldsymbol{\mathcal{R}}_b^{\mathrm{C}}$) given some metric $\boldsymbol{\mathcal{N}}$, it must also be zero in the CD system (for $\boldsymbol{\mathcal{R}}_a^{\mathrm{CD}}$ and $\boldsymbol{\mathcal{R}}_b^{\mathrm{CD}}$). That is, we have the size-intensivity condition

$$\mathcal{O}_{ab}(\boldsymbol{\mathcal{N}})^{\mathrm{C}} = 0 \implies \mathcal{O}_{ab}(\boldsymbol{\mathcal{N}})^{\mathrm{CD}} = 0. \tag{34}$$

If this condition is not fulfilled, imposing $\mathcal{O}_{ab}(\boldsymbol{\mathcal{N}})^{\mathrm{CD}} = 0$ will change $\boldsymbol{\mathcal{R}}_a^{\mathrm{CD}}$ and $\boldsymbol{\mathcal{R}}_b^{\mathrm{CD}}$ relative to $\boldsymbol{\mathcal{R}}_a^{\mathrm{C}}$ and $\boldsymbol{\mathcal{R}}_b^{\mathrm{C}}$, thereby changing the excitation energies such that $\omega_a^{\mathrm{CD}} \neq \omega_a^{\mathrm{C}}$ and $\omega_b^{\mathrm{CD}} \neq \omega_b^{\mathrm{C}}$.

Let us show that while the projected orthogonality condition is size-intensive, the non-projected condition is not, although the errors introduced appear to be small in practice. The $\boldsymbol{\mathcal{C}}_k$ vector, where $\mathcal{O}_{kl}(\boldsymbol{\mathcal{M}}) = \boldsymbol{\mathcal{C}}_k^T \boldsymbol{\mathcal{C}}_l$, can be written

$$(\boldsymbol{\mathcal{C}}_k)_\mu = \langle\mu|\Big(e^T|\mathrm{HF}\rangle R_0^k + \sum_\nu e^T|\nu\rangle R_\nu^k\Big) \equiv \langle\mu\,|\,\psi_k\rangle, \tag{35}$$

and hence

$$\mathcal{O}_{kl}(\boldsymbol{\mathcal{M}}) = \langle\psi_k\,|\,\Big(\sum_{\mu\geq 0}|\mu\rangle\langle\mu|\Big)\,|\,\psi_l\rangle \equiv \langle\psi_k\,|\,\mathcal{P}_{\mathcal{E}}\,|\,\psi_l\rangle. \tag{36}$$

Here μ in $\mathcal{P}_{\mathcal{E}}$ is restricted by the truncation of the excitation space. Note that if we define $|\psi_k\rangle = e^T|\bar{\psi}_k\rangle$, the projected condition in Eq. (20) can be cast in the same form, with $\mathcal{P}_{\mathcal{E}}$ replaced by the projection onto the space spanned by $|\bar{\psi}_a\rangle$ and $|\bar{\psi}_b\rangle$.

By the size-extensivity of T,[39] the kth eigenstate in the CD system factorizes as

$$\begin{aligned} |\psi_k^{\mathrm{CD}}\rangle &= |\psi_k^{\mathrm{C}}\rangle|\psi_0^{\mathrm{D}}\rangle \\ &= \Big(e^{T_{\mathrm{C}}}|\mathrm{HF_C}\rangle R_0^k + \sum_{\nu_{\mathrm{C}}} e^{T_{\mathrm{C}}}|\nu_{\mathrm{C}}\rangle R_{\nu_{\mathrm{C}}}^k\Big)\Big(e^{T_{\mathrm{D}}}|\mathrm{HF_D}\rangle\Big). \end{aligned} \tag{37}$$

Thus, we can write

$$\mathcal{O}_{kl}(\boldsymbol{\mathcal{M}})^{\mathrm{CD}} = \Big(\langle\psi_k^{\mathrm{C}}|\langle\psi_0^{\mathrm{D}}|\Big)\mathcal{P}_{\mathcal{E}}^{\mathrm{CD}}\Big(|\psi_l^{\mathrm{C}}\rangle|\psi_0^{\mathrm{D}}\rangle\Big). \tag{38}$$

Size-intensivity is obtained as long as there exists a $\mathcal{Z}$ such that

$$\mathcal{P}_{\mathcal{E}}^{\mathrm{CD}} = \mathcal{P}_{\mathcal{E}}^{\mathrm{C}} \otimes \mathcal{Z}, \tag{39}$$

in which case

$$\mathcal{O}_{kl}(\boldsymbol{\mathcal{M}})^{\mathrm{CD}} = \mathcal{O}_{kl}(\boldsymbol{\mathcal{M}})^{\mathrm{C}}\langle\psi_0^{\mathrm{D}}\,|\,\mathcal{Z}\,|\,\psi_0^{\mathrm{D}}\rangle. \tag{40}$$

In the untruncated limit, $\mathcal{O}_{ab}(\boldsymbol{\mathcal{M}})$ is size-intensive because

$$\mathcal{P}_{\mathcal{E}}^{\mathrm{CD}} = \mathbb{I} = \mathbb{I}_{\mathrm{C}} \otimes \mathbb{I}_{\mathrm{D}} = \mathcal{P}_{\mathcal{E}}^{\mathrm{C}} \otimes \mathcal{P}_{\mathcal{E}}^{\mathrm{D}}. \tag{41}$$

That is, $\mathcal{Z} = \mathcal{P}_{\mathcal{E}}^{\mathrm{D}}$.

No such factorization is possible for truncated excitation spaces. This is straightforward to see in particular cases. For example, in $\mathcal{P}_{\mathcal{E}}^{\mathrm{CD}}$ for CCSD, double excitations in C combine with the reference in D, giving terms of the type $|\mu_2^{\mathrm{C}}\rangle\langle\mu_2^{\mathrm{C}}| \otimes |\mathrm{HF}_{\mathrm{D}}\rangle\langle\mathrm{HF}_{\mathrm{D}}|$, while single excitations in C combine with the reference *and* single excitations in D. This gives inconsistent definitions of $\mathcal{Z}$, meaning that no such $\mathcal{Z}$ exists. In turn this means that $\mathcal{O}_{ab}(\boldsymbol{\mathcal{M}})$ is not size-intensive, a fact we confirm numerically in Section 3.

On the other hand, the size-intensivity of the projected overlap $\mathcal{O}_{ab}(\boldsymbol{\mathcal{M}}_{\boldsymbol{\mathcal{P}}})$ follows directly from the size-intensivity of $\boldsymbol{G}$ and $\boldsymbol{W}$. That is, since

$$G_{kl}^{\mathrm{CD}} = (\boldsymbol{\mathcal{R}}_k^{\mathrm{CD}})^T\boldsymbol{\mathcal{R}}_l^{\mathrm{CD}} = (\boldsymbol{\mathcal{R}}_k^{\mathrm{C}})^T\boldsymbol{\mathcal{R}}_l^{\mathrm{C}} = G_{kl}^{\mathrm{C}} \tag{42}$$

$$W_{kl}^{\mathrm{CD}} = (\boldsymbol{\mathcal{R}}_k^{\mathrm{CD}})^T\boldsymbol{\mathcal{C}}_l^{\mathrm{CD}} = (\boldsymbol{\mathcal{R}}_k^{\mathrm{C}})^T\boldsymbol{\mathcal{C}}_l^{\mathrm{C}} = W_{kl}^{\mathrm{C}}, \tag{43}$$

we get $\mathcal{O}_{ab}(\boldsymbol{\mathcal{M}}_{\boldsymbol{\mathcal{P}}})^{\mathrm{CD}} = \mathcal{O}_{ab}(\boldsymbol{\mathcal{M}}_{\boldsymbol{\mathcal{P}}})^{\mathrm{C}}$. In Eq.(43), we have used that the elements of $\boldsymbol{\mathcal{C}}_l^{\mathrm{CD}}$ that correspond to the $|\mathrm{HF_C}\rangle|\mathrm{HF_D}\rangle$ and $|\mu_{\mathrm{C}}\rangle|\mathrm{HF_D}\rangle$ blocks are identical to the vector $\boldsymbol{\mathcal{C}}_l^{\mathrm{C}}$. This is a straightforward consequence of Eqs. (35) and (37).

We now turn to the choice of the operator X_3. In this work, X_3 is chosen based on a set of requirements. These restrict the set of permissible X_3 but do not uniquely define it. The requirements are as follows.

1. To give a set of equations that is not under- or over-determined, X_3 must be uniquely specified by a single additional wavefunction parameter ζ.

2. To scale correctly with the system size, X_3 must be size-intensive. If $X_3^{\mathrm{CD}} = X_3^{\mathrm{C}}$, then $\bar{\mathcal{H}}_{\mathrm{CD}}$ separates correctly, meaning that

$$\begin{aligned} \bar{\mathcal{H}}_{\mathrm{CD}} &= e^{-X_3^{\mathrm{CD}}} \bar{H} e^{X_3^{\mathrm{CD}}} \\ &= e^{-X_3^{\mathrm{C}}} \bar{H}_{\mathrm{C}}\, e^{X_3^{\mathrm{C}}} + \bar{H}_D \\ &= \bar{\mathcal{H}}_C + \bar{H}_D. \end{aligned} \tag{44}$$

3. To imply a computational scaling of $O(M^6)$, X_3 must be factorizable. It can consist of products of single and double excitation operators, but it cannot be a connected triple excitation operator.

4. To satisfy orbital invariance, X_3 must be such that a rotation of the occupied or virtual Hartree-Fock orbitals does not imply a change in observable quantities like the energies.

5. To avoid a correction when none is needed, X_3 must become the zero operator if the states possess different symmetries. In that case, $\mathcal{O}_{ab}(\boldsymbol{\mathcal{M}}_{\boldsymbol{\mathcal{P}}}) = 0$ automatically.

6. To treat the a and b states identically, X_3 must be state invariant with respect to these states; that is, X_3 should not depend on what we designate as "state a" and "state b".

First we note that X_3 can depend on other wavefunction parameters, provided no parameters other than ζ are introduced (condition 1). In this work we let $X_3 = \zeta Z_3$, where Z_3 is

a triple excitation operator allowed to depend on the ground and excited state amplitudes. However, the wavefunction parameters that enter in Z_3 must not violate size-intensivity with respect to the C subsystem (condition 2). The only viable parameters, satisfying this criterion, are the right excited state amplitudes R^a_μ and R^b_μ; the ground state amplitudes, and the left excited state amplitudes, are *not* size-intensive. Thus, conditions 1 and 2 lead us to require the functional dependence

$$X_3(\zeta, \boldsymbol{R}_a, \boldsymbol{R}_b) = \zeta Z_3(\boldsymbol{R}_a, \boldsymbol{R}_b). \tag{45}$$

To obtain factorizability and orbital invariance (conditions 3 and 4), we construct Z_3 using products of the single and double state excitation operators

$$R^a_k = \sum_{\mu_k} R^a_{\mu_k} \tau_{\mu_k} \tag{46}$$

$$R^b_k = \sum_{\mu_k} R^b_{\mu_k} \tau_{\mu_k}, \quad k = 1, 2. \tag{47}$$

Of the possible operator products, we can construct Z_3 as a fixed linear combination of $R^a_1 R^b_2$ and $R^b_1 R^a_2$ but not of $R^a_1 R^a_2$ and $R^b_1 R^b_2$. By condition 5, the X_3 operator must tend to zero for point group transitions $G \to G'$ in which the states possess the same symmetry in G but different symmetries in G' (*e.g.*, $G = C_s$ and $G' = C_{2v}$ in H_2O). For the diagonal products, aa and bb, the Z_3 operator is totally symmetric. This implies that $\mathcal{O}_{ab}(\boldsymbol{\mathcal{M}}_{\boldsymbol{\mathcal{P}}}) = 0$ for *any* ζ when the states possess different symmetries, so there is no unique solution to the equations in G'. This is not the case for the non-diagonal terms ab and ba; Z_3 will then possess the symmetry $\Gamma_a \otimes \Gamma_b \neq A_1$. The resulting X_3 will break the symmetry of the electronic states in G' unless $\zeta = 0$. Thus, $X_3 = \zeta Z_3 = 0$ as required by condition 5.

Of such linear combinations, only the plus and minus combinations, which are unique up to an arbitrary prefactor that can be absorbed in ζ, satisfy state-invariance (condition 6).

These combinations define the operators

$$X_3^+ = \zeta(R_1^a R_2^b + R_1^b R_2^a) \tag{48}$$

$$X_3^- = \zeta(R_1^a R_2^b - R_1^b R_2^a). \tag{49}$$

Note that X_3^- vanishes at a defect, where $\boldsymbol{R}_a = \boldsymbol{R}_b$, for any ζ.

In this contribution we use X_3^-, but we do not exclude the possibility that X_3^+ could serve as a viable alternative. While an extensive study is needed to compare the performance of X_3^+ and X_3^- in general, calculations on a few systems indicate that X_3^+ gives larger deviations from CCSD in some cases (see Table S3 in the SI). We let $X_3 \equiv X_3^-$ in the following.

Summarizing, the orbital invariant SCCSD model is defined as follows. Using X_3 as given in Eq. (49), we solve the equations

$$\boldsymbol{\Omega} = 0 \tag{50}$$

$$\boldsymbol{\eta}^T + \bar{\boldsymbol{t}}^T \boldsymbol{A} = 0 \tag{51}$$

$$\boldsymbol{A}\boldsymbol{R}_a = \omega_a \boldsymbol{R}_a \tag{52}$$

$$\boldsymbol{A}\boldsymbol{R}_b = \omega_b \boldsymbol{R}_b \tag{53}$$

$$\mathcal{O}_{ab}(\boldsymbol{\mathcal{M}}_{\boldsymbol{\mathcal{P}}}) = 0 \tag{54}$$

for t_μ, $\bar{t}_\mu$, $\boldsymbol{R}_a$, $\boldsymbol{R}_b$, and ζ. All equations depend on X_3, implicitly in Eq. (54) and explicitly in the other equations. Other excited electronic states $\boldsymbol{R}_k$, where $k \neq a, b$, can be solved for separately after X_3 has been determined by Eqs. (50)–(54).

We mention that it is possible to generalize X_3 to treat several close-lying excited states. Denoting this set by $\mathcal{K}$, we can define X_3 as

$$X_3 = \sum_{m>n \in \mathcal{K}} X_3^{mn} = \sum_{m>n \in \mathcal{K}} \zeta_{mn}(R_1^m R_2^n - R_1^n R_2^m), \tag{55}$$

where X_3^{mn} is associated with the orthogonality condition $\mathcal{O}_{mn}(\boldsymbol{\mathcal{M}}_{\boldsymbol{\mathcal{P}}}) = 0$. In this case, $\mathcal{K}$ is an orthogonal set with respect to $\boldsymbol{\mathcal{M}}_{\boldsymbol{\mathcal{P}}}$, where $\boldsymbol{\mathcal{P}}$ can be taken to be the projection operator onto the span of $\mathcal{K}$.

The method can also be modified such that a subset of states $\mathcal{K}$ cannot have defects with other electronic states. In this approach, one requires for $k \in \mathcal{K}$ that

$$\boldsymbol{\mathcal{L}}_k^T = \boldsymbol{\mathcal{R}}_k^T \boldsymbol{\mathcal{M}}_{\boldsymbol{\mathcal{P}}}. \tag{56}$$

Biorthogonality of the eigenvectors of $\boldsymbol{\mathcal{A}}$ then implies that $\boldsymbol{\mathcal{R}}_k$ is orthogonal to all other right states with respect to $\boldsymbol{\mathcal{M}}_{\boldsymbol{\mathcal{P}}}$. If $\boldsymbol{\mathcal{M}}$ is used in Eq. (56), $\boldsymbol{\mathcal{L}}_k$ is similarly orthogonal to all other left states with respect to $\boldsymbol{\mathcal{M}}^{-1}$. The relation can be enforced by solving

$$\boldsymbol{\mathcal{A}}\boldsymbol{\mathcal{R}}_k = \omega_k \boldsymbol{\mathcal{R}}_k \tag{57}$$

$$\boldsymbol{\mathcal{R}}_k^T \boldsymbol{\mathcal{M}}_{\boldsymbol{\mathcal{P}}} \boldsymbol{\mathcal{A}} = \omega_k \boldsymbol{\mathcal{R}}_k^T \boldsymbol{\mathcal{M}}_{\boldsymbol{\mathcal{P}}} \tag{58}$$

using a suitable wavefunction parametrization. Further analysis and discussion of this model is deferred to a future publication.

2.2 Implementation details

The model was implemented in eT, a coupled cluster program currently under development by the authors and collaborators.[42] In this section we list programmable expressions and describe the algorithm employed to solve the equations. We use the conventional biorthonormal basis defined by[39]

$$\left|\begin{matrix} a \\ i \end{matrix}\right\rangle = E_{ai}|\mathrm{HF}\rangle, \quad \left|\begin{matrix} ab \\ ij \end{matrix}\right\rangle = E_{ai}E_{bj}|\mathrm{HF}\rangle, \tag{59}$$

and

$$\left\langle \begin{matrix} a \\ i \end{matrix} \right| = \frac{1}{2}\langle \mathrm{HF}|E_{ia}, \quad \left\langle \begin{matrix} ab \\ ij \end{matrix} \right| = \frac{1}{1+\delta_{ai,bj}}\Big(\frac{1}{3}\langle \mathrm{HF}|E_{ia}E_{jb} + \frac{1}{6}\langle \mathrm{HF}|E_{ja}E_{ib})\Big). \tag{60}$$

Expressions for the CCSD contributions to $\boldsymbol{\Omega}$ and $\boldsymbol{\eta}$, and to the $\boldsymbol{A}$ and $\boldsymbol{A}^T$ transformations, are given in the literature and will not be repeated here.[40]

To simplify, we express the triple excitation operator X_3 as in Eq. (5) using an appropriately chosen x_{ijk}^{abc} which we define below. Expressed in terms of x_{ijk}^{abc}, the corrections relative to CCSD are identical to the CCSDT[24] corrections to the single and double excitation blocks of $\boldsymbol{\Omega}$, $\boldsymbol{\eta}$, and $\boldsymbol{A}$. The $\boldsymbol{\eta}$ vector can be written

$$\eta_\nu = \langle \mathrm{HF}|[\bar{\mathcal{H}}, \tau_\nu]|\mathrm{HF}\rangle = \eta_\nu^{\mathrm{CCSD}} \tag{61}$$

since only T_1 contributes. For the $\boldsymbol{\Omega}$ vector we have

$$\begin{aligned} \Omega_\mu &= \langle \mu|\bar{\mathcal{H}}|\mathrm{HF}\rangle \\ &= \langle \mu|\bar{H}|\mathrm{HF}\rangle + \langle \mu|[\hat{H}, X_3]|\mathrm{HF}\rangle \\ &= \Omega_\mu^{\mathrm{CCSD}} + \Delta\Omega_\mu, \end{aligned} \tag{62}$$

where $\hat{H} = e^{-T_1}He^{T_1}$ is the T_1-transformed Hamiltonian. We express $\hat{H}$ as

$$\hat{H} = \sum_{pq} h_{pq}E_{pq} + \frac{1}{2}\sum_{pqrs} g_{pqrs}(E_{pq}E_{rs} - \delta_{qr}E_{ps}) + h_{\mathrm{nuc}}. \tag{63}$$

The electron repulsion integrals, g_{pqrs}, are constructed from the Cholesky vectors obtained using the implementation described by Folkestad *et al.*[43] The single and double excitation corrections to $\boldsymbol{\Omega}$ are given by

$$\Delta\Omega_{ai} = \sum_{bjck}(x_{ijk}^{abc} - x_{kji}^{abc})L_{jbkc}, \tag{64}$$

where $L_{jbkc} = 2g_{jbkc} - g_{jckb}$, and

$$\begin{aligned}\Delta\Omega_{aibj} = \frac{1}{1+\delta_{ai,bj}} \mathscr{P}_{ij}^{ab} \Big(& \sum_{ck} (x_{ijk}^{abc} - x_{ikj}^{abc}) F_{kc} \\ & + \sum_{ckl} (x_{lkj}^{bac} + x_{jlk}^{bac} - 2x_{jkl}^{bac}) g_{lcki} \\ & + \sum_{cdk} (2x_{jik}^{bcd} - x_{kij}^{bcd} - x_{jki}^{bcd}) g_{ackd} \Big).\end{aligned} \tag{65}$$

Here, F_{pq} is the Fock matrix expressed using T_1-transformed integrals h_{pq} and g_{pqrs}, and $\mathscr{P}_{ij}^{ab}$ is defined by

$$\mathscr{P}_{ij}^{ab} Y_{ij}^{ab} = Y_{ij}^{ab} + Y_{ji}^{ba}. \tag{66}$$

The elements of $\boldsymbol{A}$ can be expressed as $A_{\mu\nu} = \langle \mu | [\bar{\mathcal{H}}, \tau_\nu] | \mathrm{HF} \rangle$, giving

$$\begin{aligned}\boldsymbol{A} &= \boldsymbol{A}^{\mathrm{CCSD}} + \Delta\boldsymbol{A} \\ &= \boldsymbol{A}^{\mathrm{CCSD}} + \begin{pmatrix} 0 & 0 \\ \langle \mu_2 | [[\hat{H}, X_3], \tau_{\nu_1}] | \mathrm{HF} \rangle & 0 \end{pmatrix},\end{aligned} \tag{67}$$

where we have written the matrix in terms of the blocks given by $\{\langle \mu_1 |, \langle \mu_2 |\}$ and $\{|\nu_1\rangle, |\nu_2\rangle\}$. Defining $\Delta\boldsymbol{\rho} = (\Delta\boldsymbol{A})\boldsymbol{c}$, we get $\Delta\rho_{ai} = 0$ while $\Delta\rho_{aibj}$ may be obtained from the expression for $\Delta\Omega_{aibj}$ by redefining the integrals in Eq. (65). In particular,

$$F_{kc} \mapsto X_{kc} = \sum_{dl} c_{dl}\, L_{ldkc} \tag{68}$$

$$g_{lcki} \mapsto Y_{lcki} = \sum_{d} g_{lckd}\, c_{di} \tag{69}$$

$$g_{ackd} \mapsto Z_{ackd} = -\sum_{l} c_{al}\, g_{lckd}. \tag{70}$$

For the left transformation, $\Delta\boldsymbol{\sigma} = \boldsymbol{b}^T(\Delta\boldsymbol{A})$, we have

$$\begin{aligned}\Delta\sigma_{ck} = &\sum_{dlemfn} (x^{def}_{lmn} - x^{def}_{lnm}) b_{dlem} L_{kcnf} \\ &+ \sum_{dlemfn} (x^{def}_{mln} + x^{def}_{lnm} - 2x^{def}_{lmn}) b_{dlcn} g_{mekf} \\ &+ \sum_{dlemfn} (x^{def}_{lnm} + x^{def}_{nml} - 2x^{def}_{lmn}) b_{dlek} g_{mcnf}\end{aligned} \tag{71}$$

and $\Delta\sigma_{aibj} = 0$.

Finally, we define x^{abc}_{ijk}. The implemented expressions exploit the factorization of X_3 in Eqs. (64), (65), and (71) to give $O(M^6)$ computational scaling. Defining $\tilde{R}^n_{bjck} = R^n_{bjck}(1 + \delta_{bj,ck})$, we can write the product operator $R^m_1 R^n_2$ as

$$\begin{aligned}R^m_1 R^n_2 &= \sum_{ai} R^m_{ai} E_{ai} \sum_{bj \geq ck} R^n_{bjck} E_{bj} E_{ck} \\ &= \frac{1}{2} \sum_{aibjck} R^m_{ai} \tilde{R}^n_{bjck} E_{ai} E_{bj} E_{ck}.\end{aligned} \tag{72}$$

Because $\{E_{ai}\}$ commutes, we furthermore have

$$R^m_1 R^n_2 = \frac{1}{6} \sum_{aibjck} \Big(\frac{1}{2} \mathscr{P}^{abc}_{ijk} (R^m_{ai} \tilde{R}^n_{bjck}) \Big) E_{ai} E_{bj} E_{ck}, \tag{73}$$

where

$$\begin{aligned}\mathscr{P}^{abc}_{ijk} Y^{abc}_{ijk} = &Y^{abc}_{ijk} + Y^{acb}_{ikj} + Y^{bac}_{jik} \\ &+ Y^{bca}_{jki} + Y^{cab}_{kij} + Y^{cba}_{kji}.\end{aligned} \tag{74}$$

Comparison of Eqs. (49) and (73) thus implies that

$$x^{abc}_{ijk} = \frac{\zeta}{2} \mathscr{P}^{abc}_{ijk} (R^a_{ai} \tilde{R}^b_{bjck} - R^b_{ai} \tilde{R}^a_{bjck}) \tag{75}$$

Using the $bj \leftrightarrow ck$ symmetry of $\tilde{R}^a_{bjck}$ and $\tilde{R}^b_{bjck}$, the number of terms arising from Eq. (75) can be reduced by a factor of two. The implementation includes routines that compute the contributions in Eqs. (64), (65), and (71) for an y^{abc}_{ijk} defined by

$$\begin{aligned} y^{abc}_{ijk} &= \frac{\zeta}{2} \mathscr{P}^{abc}_{ijk} (U_{ai} V_{bjck}) \\ &= \zeta (U_{ai} V_{bjck} + U_{ck} V_{aibj} + U_{bj} V_{ckai}). \end{aligned} \tag{76}$$

To compute the entire correction resulting from the amplitudes x^{abc}_{ijk} given in Eq. (75), these routines are called twice using appropriately defined $\boldsymbol{U}$ and $\boldsymbol{V}$.

To derive the overlap in the biorthonormal basis, we introduce an orthonormal basis that relates the bra and ket vectors in Eqs. (59) and (60), where we also include the reference bra and ket, $\langle \mathrm{HF}|$ and $|\mathrm{HF}\rangle$. To distinguish the different vectors, we denote the kets in Eq. (59) as $|\mu\rangle$ and the bras in Eq. (60) as $\langle\tilde{\mu}|$, with $\mu \geq 0$. From the Cholesky decomposition

$$\mathcal{S}_{\mu\nu} = \langle \mu \,|\, \nu \rangle = (\boldsymbol{\mathcal{L}} \boldsymbol{\mathcal{L}}^T)_{\mu\nu}, \tag{77}$$

we define the orthonormal basis

$$|\bar{\mu}\rangle \equiv \sum_\nu \mathcal{L}^{-1}_{\mu\nu} |\nu\rangle = \sum_\nu \mathcal{L}^T_{\mu\nu} |\tilde{\nu}\rangle. \tag{78}$$

If we express the equations in this orthonormal basis, we can translate to the biorthonormal basis using Eq. (78). Denoting the matrices in the biorthonormal and orthonormal bases by $\boldsymbol{\mathcal{X}}$ and $\bar{\boldsymbol{\mathcal{X}}}$, respectively, we have

$$\begin{aligned} \bar{\mathcal{X}}_{\mu\nu} &= \langle \bar{\mu} \,|\, X \,|\, \bar{\nu} \rangle \\ &= \sum_{\sigma\theta} \mathcal{L}^T_{\mu\sigma} \langle \tilde{\sigma} \,|\, X \,|\, \theta \rangle \mathcal{L}^{-1}_{\nu\theta} \\ &= (\boldsymbol{\mathcal{L}}^T \boldsymbol{\mathcal{X}} \, \boldsymbol{\mathcal{L}}^{-T})_{\mu\nu}, \end{aligned} \tag{79}$$

and so

$$\bar{\boldsymbol{\mathcal{A}}} = \boldsymbol{\mathcal{L}}^T \boldsymbol{\mathcal{A}} \boldsymbol{\mathcal{L}}^{-T}, \quad \bar{\boldsymbol{\mathcal{Q}}} = \boldsymbol{\mathcal{L}}^T \boldsymbol{\mathcal{Q}} \boldsymbol{\mathcal{L}}^{-T}. \tag{80}$$

The right eigenvectors of $\boldsymbol{\mathcal{A}}$ and $\bar{\boldsymbol{\mathcal{A}}}$ are thus related as $\bar{\boldsymbol{\mathcal{R}}} = \boldsymbol{\mathcal{L}}^T \boldsymbol{\mathcal{R}}$, implying that

$$\begin{aligned} \mathcal{O}_{kl}(\boldsymbol{\mathcal{M}}) &= \bar{\boldsymbol{\mathcal{R}}}_k^T \bar{\boldsymbol{\mathcal{Q}}}^T \bar{\boldsymbol{\mathcal{Q}}} \bar{\boldsymbol{\mathcal{R}}}_l \\ &= \boldsymbol{\mathcal{R}}_k^T \boldsymbol{\mathcal{Q}}^T \boldsymbol{\mathcal{S}} \boldsymbol{\mathcal{Q}} \boldsymbol{\mathcal{R}}_l. \end{aligned} \tag{81}$$

Furthermore, since

$$\boldsymbol{\mathcal{S}} = \begin{pmatrix} 1 & \mathbf{0} \\ \mathbf{0} & \boldsymbol{S} \end{pmatrix}, \tag{82}$$

we can also write

$$\begin{aligned} \mathcal{O}_{kl}(\boldsymbol{\mathcal{M}}) =& R_k^0 R_l^0 (1 + \boldsymbol{q}^T \boldsymbol{S} \boldsymbol{q}) + R_k^0 \boldsymbol{q}^T \boldsymbol{S} \boldsymbol{Q} \boldsymbol{R}_l \\ &+ \boldsymbol{R}_k^T \boldsymbol{Q}^T \boldsymbol{S} \boldsymbol{q} R_l^0 + \boldsymbol{R}_k^T \boldsymbol{Q}^T \boldsymbol{S} \boldsymbol{Q} \boldsymbol{R}_l. \end{aligned} \tag{83}$$

Similarly, we have

$$\mathcal{O}_{kl}(\boldsymbol{\mathcal{M}}_{\boldsymbol{\mathcal{P}}}) = \sum_{m,n=a,b} \bar{W}_{km}^T \bar{G}_{mn}^{-1} \bar{W}_{nl} \tag{84}$$

where

$$\bar{G}_{kl} = \bar{\boldsymbol{\mathcal{R}}}_k^T \bar{\boldsymbol{\mathcal{R}}}_l = \boldsymbol{\mathcal{R}}_k^T \boldsymbol{\mathcal{S}} \boldsymbol{\mathcal{R}}_l \tag{85}$$

$$\bar{W}_{kl} = \bar{\boldsymbol{\mathcal{R}}}_k^T \bar{\boldsymbol{\mathcal{Q}}} \bar{\boldsymbol{\mathcal{R}}}_l = \boldsymbol{\mathcal{R}}_k^T \boldsymbol{\mathcal{S}} \boldsymbol{\mathcal{Q}} \boldsymbol{\mathcal{R}}_l. \tag{86}$$

Using the block-structure of $\boldsymbol{\mathcal{S}}, \boldsymbol{\mathcal{Q}}, \boldsymbol{\mathcal{R}}_k$, and $\boldsymbol{\mathcal{R}}_l$, we can write

$$\bar{G}_{kl} = R_k^0 R_l^0 + \boldsymbol{R}_k^T \boldsymbol{S} \boldsymbol{R}_l \tag{87}$$

$$\bar{W}_{kl} = R_k^0 R_l^0 + (\boldsymbol{R}_k^T \boldsymbol{S} \boldsymbol{q}) R_l^0 + \boldsymbol{R}_k^T \boldsymbol{S} \boldsymbol{Q} \boldsymbol{R}_l. \tag{88}$$

The $\boldsymbol{q}$ vector is given by

$$q_{ai} = t_i^a \tag{89}$$

$$q_{aibj} = \frac{1}{1 + \delta_{ai,bj}} (t_{ij}^{ab} + t_i^a t_j^b), \tag{90}$$

and the $\boldsymbol{S}$, $\boldsymbol{Q}$, and $\boldsymbol{Q}^T$ transformations are given by

$$\rho_{ai} = (\boldsymbol{Q}\boldsymbol{c})_{ai} = c_{ai} \tag{91}$$

$$\rho_{aibj} = (\boldsymbol{Q}\boldsymbol{c})_{aibj} = c_{aibj} + \frac{1}{1 + \delta_{ai,bj}} (c_{ai} t_j^b + c_{bj} t_i^a) \tag{92}$$

$$\sigma_{ai} = (\boldsymbol{b}^T \boldsymbol{Q})_{ai} = b_{ai} + \sum_{ck} t_k^c b_{aick} \tag{93}$$

$$\sigma_{aibj} = (\boldsymbol{b}^T \boldsymbol{Q})_{aibj} = b_{aibj} \tag{94}$$

$$\rho_{ai} = (\boldsymbol{S}\boldsymbol{c})_{ai} = 2c_{ai} \tag{95}$$

$$\rho_{aibj} = (\boldsymbol{S}\boldsymbol{c})_{aibj} = 2(1 + \delta_{ai,bj})(2c_{aibj} - c_{ajbi}). \tag{96}$$

To solve the equations simultaneously, we employ a direct inversion in the iterative subspace (DIIS)[44] algorithm on the residuals in Eqs. (50)–(54). The residuals in Eqs. (50)–(53) are preconditioned using the diagonal orbital differences approximation of $\boldsymbol{A}$. For details regarding this preconditioner and its use in coupled cluster theory, we refer the reader to the literature.[39,45] No preconditioner is applied to the orthogonality condition in Eq. (54). To update ζ, we apply DIIS to minimize the averaged overlap using an update estimate given by $\zeta + \Delta\zeta$, where $\Delta\zeta = -\mathcal{O}_{ab}(\boldsymbol{\mathcal{M}}_{\boldsymbol{\mathcal{P}}})$. Computing the derivative of $\mathcal{O}_{ab}(\boldsymbol{\mathcal{M}}_{\boldsymbol{\mathcal{P}}})$ with respect to ζ, as was done numerically in Ref. 32, can be used to improve this updating scheme.

3 Results and discussion

First we reconsider the intersection seam between the first two A'-excited states ($1^1A'$, $2^1A'$) in hypofluorous acid (HOF) investigated in our previous papers.[23,32] In Figures 1 and 2 we compare the CCSD and SCCSD branching planes at the intersection point $\boldsymbol{R}_0$ in the plane where the OH bond length is 1.090 Å.

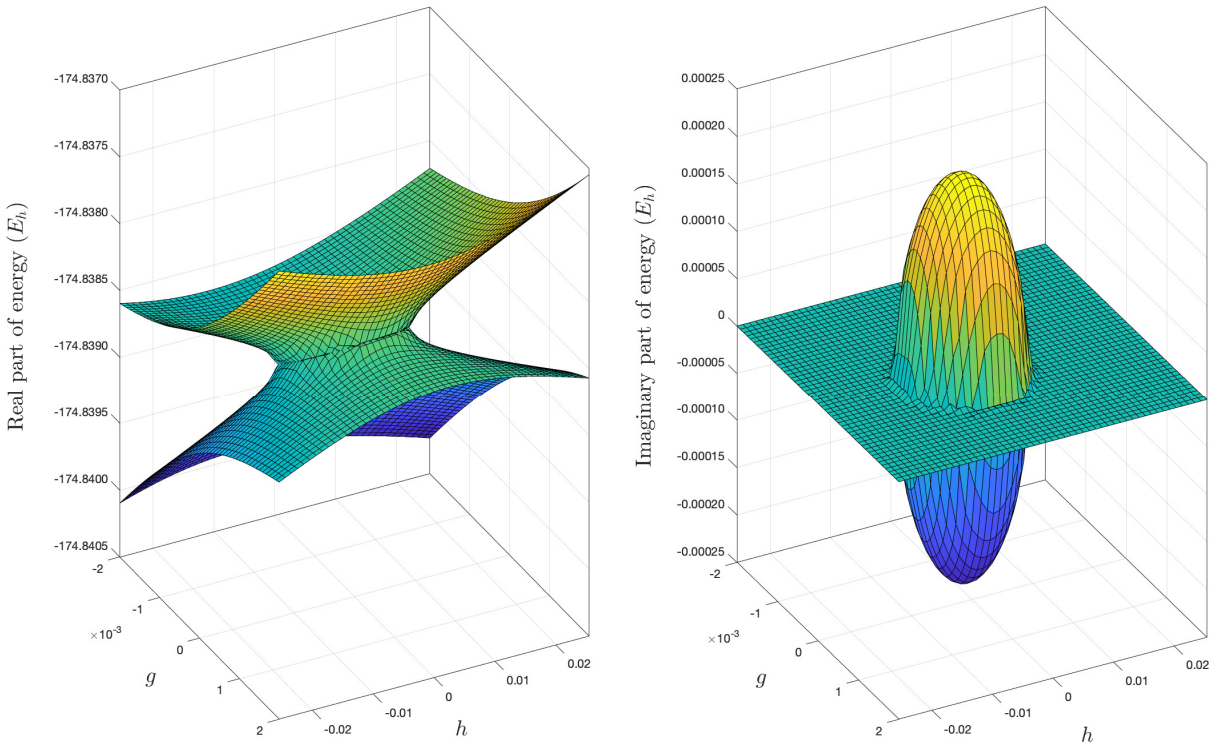

Figure 1: $1^1A'/2^1A'$ CCSD/aug-cc-pVDZ branching plane in HOF. Given is the real part (left) and the imaginary part (right) of the energies.

The findings are consistent with earlier work.[22,23,32] The CCSD intersection points form an approximately elliptical shape in the branching plane with pairs of complex energies in the interior of the ellipse (see Figure 1). In the three-dimensional internal coordinate space, this translates to a cylindrically shaped intersection seam, as demonstrated and explained previously.[23] In contrast, the SCCSD energy surfaces are conically shaped in the branching plane with a single intersection point (see Figure 2), just as for the single-excitation model.[32] This translates to a correct one-dimensional seam in the internal coordinate space ($N - 2 =$

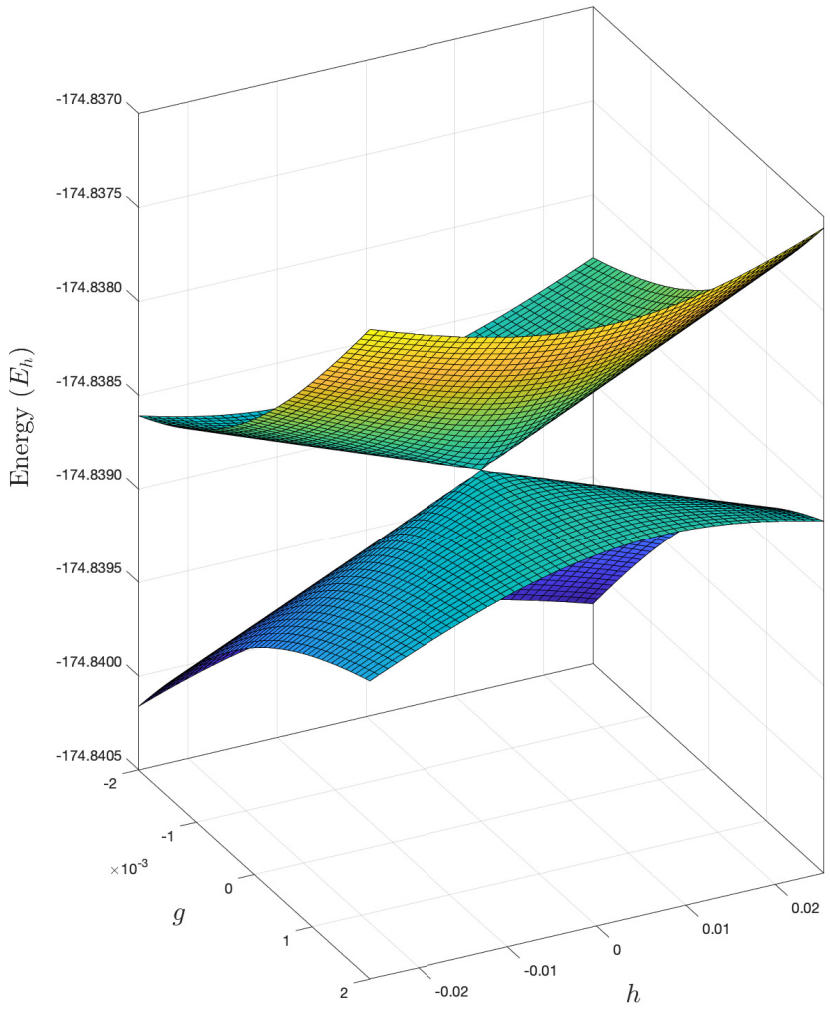

Figure 2: $1^1A'/2^1A'$ SCCSD/aug-cc-pVDZ branching plane in HOF.

1). In Figure 3 we map out parts of this intersection seam, demonstrating that it is is a curve. The point $(g, h) = (0, 0)$ in Figure 2 is the intersection point in the OH-slice in Figure 3 for which $R_{\mathrm{OH}} = 1.090$ Å.

The $\boldsymbol{g}$ and $\boldsymbol{h}$ vectors, and the seam vector $\boldsymbol{s}$, were determined using internal coordinates obtained from a normal mode Hartree-Fock calculation at $\boldsymbol{R}_0$ using QChem.[46] Details are given in the SI. In this work we use orthonormalized non-mass-weighted normal modes, which correctly preserve the molecule's center of mass, not the mass-weighted normal modes used

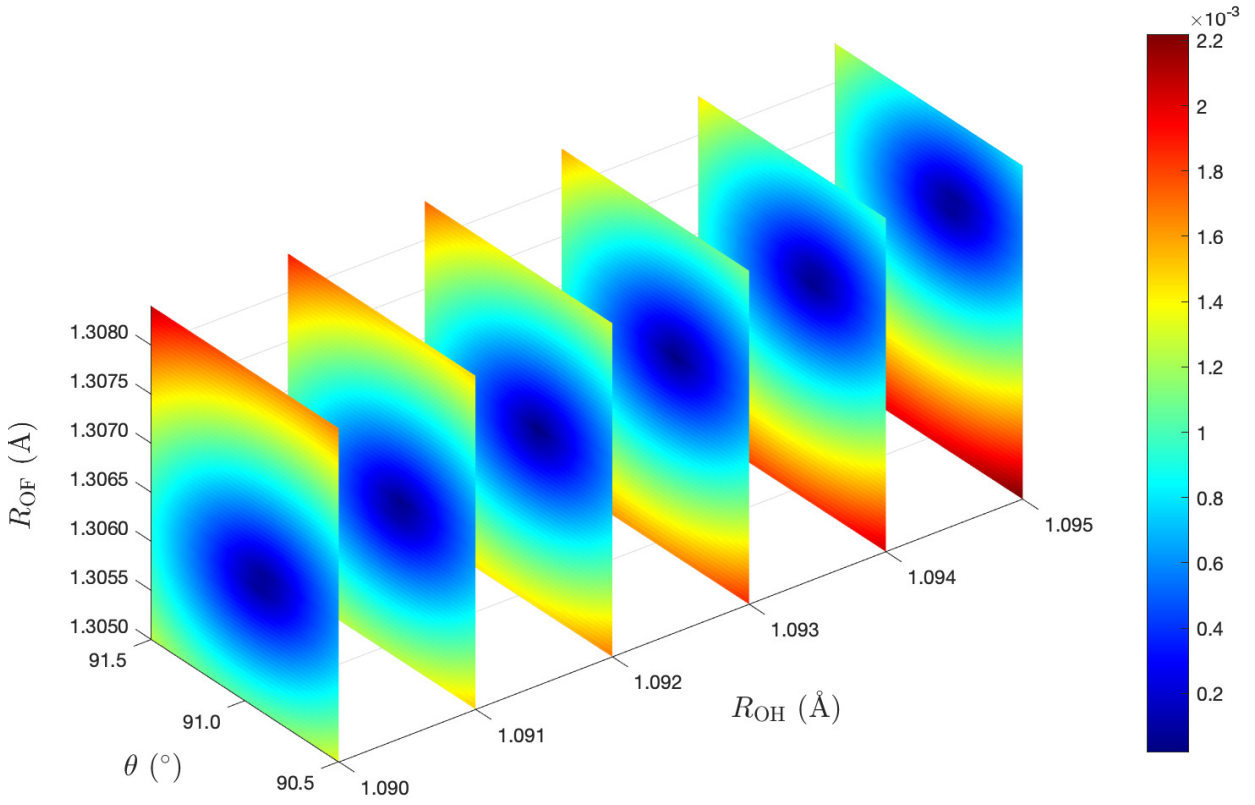

Figure 3: $1^1A'/2^1A'$ SCCSD/aug-cc-pVDZ intersection seam. The coloring shows the energy difference between the two states in Hartree. Here θ denotes the H−O−F angle, while R_{OH} and R_{OF} are the OH and OF bond distances, respectively.

in Ref. 32. Qualitatively, the results are not affected by this; in particular, the branching plane in Figure 2 exhibits the same features as Figure 3 in Ref. 32.

To show that the projected condition $\mathcal{O}_{ab}(\boldsymbol{\mathcal{M}}_{\boldsymbol{\mathcal{P}}}) = 0$ satisfies size-intensivity, we have performed calculations on a non-interacting CD system consisting of a formaldehyde molecule (C) and n He atoms, $n = 1, 2, 3, 4, 8$ (D). These atoms are positioned at a distance of 200 Å from formaldehyde, making their interaction with formaldehyde negligible. We also include numbers for the non-projected condition $\mathcal{O}_{ab}(\boldsymbol{\mathcal{M}}) = 0$ to illustrate the errors obtained in that case. In Table 1, we compare excitation energies for the $1\,^1A_1$ and $2\,^1A_1$ states using $\mathcal{O}_{ab}(\boldsymbol{\mathcal{M}}_{\boldsymbol{\mathcal{P}}})$ and $\mathcal{O}_{ab}(\boldsymbol{\mathcal{M}})$. As expected, no inconsistency errors arise using the projected condition $\mathcal{O}_{ab}(\boldsymbol{\mathcal{M}}_{\boldsymbol{\mathcal{P}}}) = 0$ while non-zero deviations result from using $\mathcal{O}_{ab}(\boldsymbol{\mathcal{M}}) = 0$. The results verify numerically the proof of intensivity for $\mathcal{O}_{ab}(\boldsymbol{\mathcal{M}}_{\boldsymbol{\mathcal{P}}}) = 0$; see Eqs. (42) and (43)

Table 1: Excitation energies ω_k and discrepancies $\Delta\omega_k$, $k = a, b$, for the non-projected ($\boldsymbol{\mathcal{M}}$) and projected ($\boldsymbol{\mathcal{M}}_{\boldsymbol{\mathcal{P}}}$) orthogonality conditions on $CH_2O(He)_n$. All He atoms are placed at a distance of about 200 Å from CH_2O. Energies are in units of Hartree. Energies and residuals were converged using a threshold equal to 10^{-11}. The CH_2O geometry is given in the SI.

Method	n	ω_a	$\Delta\omega_a$	ω_b	$\Delta\omega_b$
SCCSD($\boldsymbol{\mathcal{M}}$)	0	0.29396556345	–	0.30073161296	–
	1	0.29396557140	8.0×10^{-9}	0.30073164810	3.5×10^{-8}
	2	0.29396557935	1.6×10^{-8}	0.30073168325	7.0×10^{-8}
	3	0.29396558730	2.4×10^{-8}	0.30073171839	1.1×10^{-7}
	4	0.29396559525	3.2×10^{-8}	0.30073175353	1.4×10^{-7}
	8	0.29396562704	6.4×10^{-8}	0.30073189406	2.8×10^{-7}
SCCSD($\boldsymbol{\mathcal{M}}_{\boldsymbol{\mathcal{P}}}$)	0	0.29396403184	–	0.30072483930	–
	1	0.29396403184	$< 10^{-11}$	0.30072483930	$< 10^{-11}$
	2	0.29396403184	$< 10^{-11}$	0.30072483930	$< 10^{-11}$
	3	0.29396403184	$< 10^{-11}$	0.30072483930	$< 10^{-11}$
	4	0.29396403184	$< 10^{-11}$	0.30072483930	$< 10^{-11}$
	8	0.29396403184	$< 10^{-11}$	0.30072483930	$< 10^{-11}$
CCSD	0	0.29375048778	-	0.29969409128	-

and the surrounding text. They also confirm the non-intensivity of $\mathcal{O}_{ab}(\boldsymbol{\mathcal{M}}) = 0$, which is found to give errors that increase linearly with the number of He atoms (see Figure 5). The errors introduced using the non-projected overlap $\mathcal{O}_{ab}(\boldsymbol{\mathcal{M}}) = 0$ are small ($< 10^{-6}$ Hartree), so they might not be important in practice. Nevertheless, given the energy consistency that is guaranteed by it, the projected condition $\mathcal{O}_{ab}(\boldsymbol{\mathcal{M}}_{\boldsymbol{\mathcal{P}}}) = 0$ appears preferable.

We have reinvestigated the known defect in formaldehyde as well.[22,32] For details regarding the geometry, we refer the reader to the original study by Köhn and Tajti.[22] Again, the

Table 2: Single-point excitation energies. We use the aug-cc-pVDZ basis and a 10^{-6} residual threshold. The excited states are listed as a and b, with associated excitation energies ω_a and ω_b given in eV. The metric used in the SCCSD calculations is denoted by $\boldsymbol{\mathcal{M}}$ and $\boldsymbol{\mathcal{M}}_{\boldsymbol{\mathcal{P}}}$. Geometries are in the SI.

	a	b	ω_a^{CCSD}	$\omega_a(\boldsymbol{\mathcal{M}})$	$\omega_a(\boldsymbol{\mathcal{M}}_{\boldsymbol{\mathcal{P}}})$	ω_b^{CCSD}	$\omega_b(\boldsymbol{\mathcal{M}})$	$\omega_b(\boldsymbol{\mathcal{M}}_{\boldsymbol{\mathcal{P}}})$
Ammonia	1^1A_1	2^1A_1	5.9372	5.9376	5.9379	9.3400	9.3401	9.3401
Water	1^1B_1	2^1B_1	7.4104	7.4078	7.4077	11.0739	11.0749	11.0749
	1^1A_1	2^1A_1	9.9436	9.9368	9.9357	11.7632	11.7740	11.7756
Uracil	$1^1A''$	$2^1A''$	5.1285	5.1276	5.1276	6.0073	6.0073	6.0073
Thymine	$1^1A''$	$2^1A''$	5.3086	5.3069	5.3069	5.7934	5.7933	5.7933
Glycine	$1^1A'$	$2^1A'$	6.4401	6.4400	6.4400	7.2609	7.2610	7.2610
Butanal	$1^1A'$	$2^1A'$	6.7083	6.7079	6.7079	7.4199	7.4184	7.4184

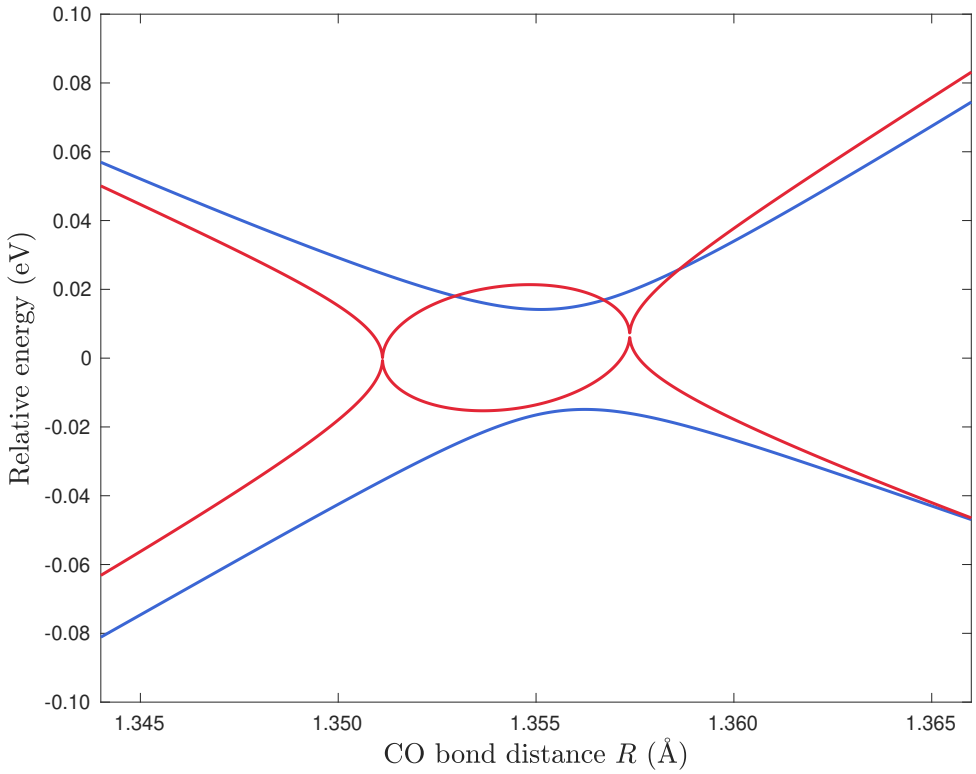

Figure 4: Relative $1\,^1A_1$ and $2\,^1A_1$ excited state SCCSD (blue) and CCSD (red) energies for formaldehyde using aug-cc-pVDZ. For CCSD, the energy $E_k = \mathrm{Re}E_k + i\mathrm{Im}E_k$ of the kth state is represented as $E_k = \mathrm{Re}E_k + \mathrm{Im}E_k$, where $k = 1, 2$.

numbers, shown in Figure 4, are consistent with earlier findings. The defective region is replaced by an avoided crossing, as expected; two coordinates needs to be varied to find an intersection point.[32] For all CO bond lengths, the correction relative to the real part of the CCSD energies stays below 0.05 eV. They are thus smaller than the usual error of CCSD within its domain of validity, approximately ≤ 0.10 eV.[47] This is also the case for HOF. The real part of the CCSD-SCCSD energy difference in the branching plane in Figures 1 and 2 is less than 0.01 eV. We emphasize that although the cited 0.10 eV error range is a convenient measure of the magnitude of the SCCSD-CCSD deviation, the CCSD errors may be larger or smaller depending on such factors as the degree of multireference character in the ground state and the proximity to a defective intersection seam.

Finally, we have performed single-point calculations on a set of molecules using the pro-

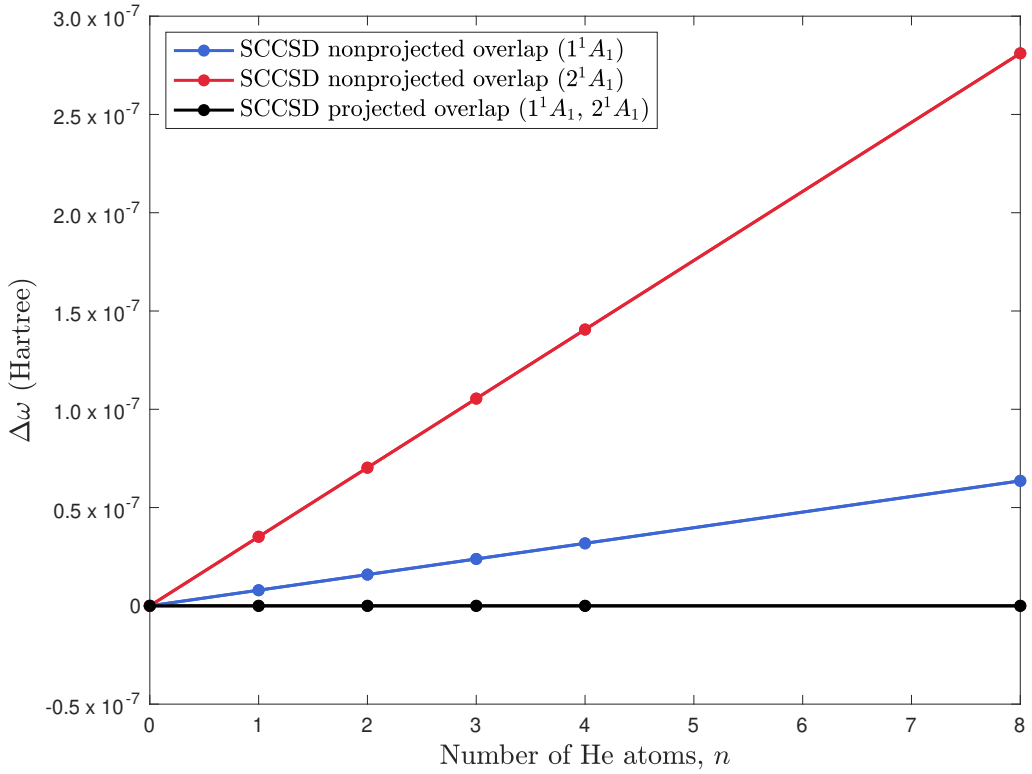

Figure 5: Deviations $\Delta\omega$ in SCCSD/aug-cc-pVDZ excitation energies of $CH_2O(He)_n$ relative to a calculation on an isolated CH_2O. Obtained $\Delta\omega$ are shown both using $\boldsymbol{\mathcal{M}}$ (labelled 'non-projected overlap') and $\boldsymbol{\mathcal{M}}_{\boldsymbol{\mathcal{P}}}$ ('projected overlap'). The He atoms are distanced sufficiently far away from CH_2O (200 Å) to be non-interacting to within 10^{-11} Hartree in the CCSD and projected SCCSD energies.

jected and non-projected orthogonality conditions (see Table 2). These calculations provide some indication of the SCCSD-CCSD deviation in regions of the potential energy surfaces where the electronic states are not nearly degenerate. From Table 2 we see that the deviations are less than 0.02 eV in all cases, and that the non-projected and projected energies are more similar to each other than to CCSD. Note also that the comparatively small magnitude of the energy deviations in Table 2 is expected. Overlaps between states in CCSD are often close to zero when the energy difference is large.

4 Concluding remarks

In this work we have shown that the similarity constrained approach admits a formulation at the CCSD level of theory that is orbital invariant, size-intensive, and unique for a chosen pair of electronic excited states. Preliminary calculations indicate that the correction relative to CCSD falls within the commonly observed error range of CCSD. Future developments needed for coupled cluster dynamics include molecular gradients and nonadiabatic coupling elements, as well as generalizations of the model to other levels in the coupled cluster hierarchy. Given the expensive nature of dynamics simulations, we are currently looking into a less expensive perturbative doubles SCC2 method based on the well-established CC2[26] method.

Acknowledgement

We thank Franco Egidi for helpful discussions, and Sarai D. Folkestad for providing useful comments on the manuscript. We also acknowledge discussions with Rolf H. Myhre. We acknowledge funding from the Marie Skłodowska-Curie European Training Network through grant agreement no. 765739 (COSINE) and the Norwegian Research Council grants CCGPU (no. 263110) and TheoLight (no. 275506). H.K. acknowledges the Otto Mønsted Fond and E.F.K. acknowledges Fondet til professor Leif Tronstads minne. We acknowledge computer resources from NOTUR through project no. nn2962k.

Supporting Information Available

Branching plane coordinates, normal modes, and intersection geometry, as well as grid-sizes and interpolation specifications for the branching plane and seam heat maps for hypofluorous acid calculations, calculations using the X_3^+ combination, along with geometries used in single-point calculations.

References

(1) Zhu, X.; Yarkony, D. R. Non-adiabaticity: the importance of conical intersections. *Mol. Phys.* **2016**, *114*, 1983–2013.

(2) Born, M.; Oppenheimer, R. Zur Quantentheorie der Molekeln. *Ann. Phys.* **1927**, *389*, 457–484.

(3) Crespo-Otero, R.; Barbatti, M. Recent Advances and Perspectives on Nonadiabatic Mixed Quantum–Classical Dynamics. *Chem. Rev.* **2018**, *118*, 7026–7068.

(4) Curchod, B. F. E.; Martínez, T. J. Ab Initio Nonadiabatic Quantum Molecular Dynamics. *Chem. Rev.* **2018**, *118*, 3305–3336.

(5) Tully, J. C.; Preston, R. K. Trajectory Surface Hopping Approach to Nonadiabatic Molecular Collisions: The Reaction of H+ with D2. *J. Chem. Phys.* **1971**, *55*, 562–572.

(6) Tully, J. C. Molecular dynamics with electronic transitions. *J. Chem. Phys.* **1990**, *93*, 1061–1071.

(7) Ben-Nun, M.; Quenneville, J.; Martinez, T. J. Ab Initio Multiple Spawning: Photochemistry from First Principles Quantum Molecular Dynamics. *J. Phys. Chem. A* **2000**, *104*, 5161–5175.

(8) Ben-Nun, M.; Martínez, T. J. *Adv. Chem. Phys.*; John Wiley & Sons, Ltd, 2002; pp 439–512.

(9) Makhov, D. V.; Symonds, C.; Fernandez-Alberti, S.; Shalashilin, D. V. Ab initio quantum direct dynamics simulations of ultrafast photochemistry with Multiconfigurational Ehrenfest approach. *Chem. Phys.* **2017**, *493*, 200 – 218.

(10) Beck, M.; Jäckle, A.; Worth, G.; Meyer, H.-D. The multiconfiguration time-dependent Hartree (MCTDH) method: a highly efficient algorithm for propagating wavepackets. *Phys. Rep.* **2000**, *324*, 1 – 105.

(11) Koch, H.; Jørgensen, P. Coupled cluster response functions. *J. Chem. Phys.* **1990**, *93*, 3333–3344.

(12) Stanton, J. F.; Bartlett, R. J. The equation of motion coupled-cluster method. A systematic biorthogonal approach to molecular excitation energies, transition probabilities, and excited state properties. *J. Chem. Phys.* **1993**, *98*, 7029–7039.

(13) Krylov, A. I. Equation-of-Motion Coupled-Cluster Methods for Open-Shell and Electronically Excited Species: The Hitchhiker's Guide to Fock Space. *Annu. Rev. Phys. Chem.* **2008**, *59*, 433–462.

(14) Stanton, J. F. Many-body methods for excited state potential energy surfaces. I. General theory of energy gradients for the equation-of-motion coupled-cluster method. *J. Chem. Phys.* **1993**, *99*, 8840–8847.

(15) Koch, H.; Jensen, H. J. A.; Jørgensen, P.; Helgaker, T.; Scuseria, G. E.; Schaefer, H. F. Coupled cluster energy derivatives. Analytic Hessian for the closed-shell coupled cluster singles and doubles wave function: Theory and applications. *J. Chem. Phys.* **1990**, *92*, 4924–4940.

(16) Christiansen, O. First-order nonadiabatic coupling matrix elements using coupled cluster methods. I. Theory. *J. Chem. Phys.* **1999**, *110*, 711–723.

(17) Ichino, T.; Gauss, J.; Stanton, J. F. Quasidiabatic states described by coupled-cluster theory. *J. Chem. Phys.* **2009**, *130*, 174105.

(18) Tajti, A.; Szalay, P. G. Analytic evaluation of the nonadiabatic coupling vector between excited states using equation-of-motion coupled-cluster theory. *J. Chem. Phys.* **2009**, *131*, 124104.

(19) Faraji, S.; Matsika, S.; Krylov, A. I. Calculations of non-adiabatic couplings within equation-of-motion coupled-cluster framework: Theory, implementation, and validation against multi-reference methods. *J. Chem. Phys.* **2018**, *148*, 044103.

(20) Purvis, G. D.; Bartlett, R. J. A full coupled-cluster singles and doubles model: The inclusion of disconnected triples. *J. Chem. Phys.* **1982**, *76*, 1910–1918.

(21) Hättig, C. In *Response Theory and Molecular Properties (A Tribute to Jan Linderberg and Poul Jørgensen)*; Jensen, H., Ed.; Advances in Quantum Chemistry; Academic Press, 2005; Vol. 50; pp 37 – 60.

(22) Kohn, A.; Tajti, A. Can coupled-cluster theory treat conical intersections? *J. Chem. Phys.* **2007**, *127*, 044105.

(23) Kjønstad, E. F.; Myhre, R. H.; Martínez, T. J.; Koch, H. Crossing conditions in coupled cluster theory. *J. Chem. Phys.* **2017**, *147*, 164105.

(24) Noga, J.; Bartlett, R. J. The full CCSDT model for molecular electronic structure. *J. Chem. Phys.* **1987**, *86*, 7041–7050.

(25) Noga, J.; Bartlett, R. Erratum: The full CCSDT model for molecular electronic structure [J. Chem. Phys. 8 6, 7041 (1987)]. *J. Chem. Phys.* **1988**, *89*, 3401–3401.

(26) Christiansen, O.; Koch, H.; Jørgensen, P. The second-order approximate coupled cluster singles and doubles model CC2. *Chem. Phys. Letters* **1995**, *243*, 409 – 418.

(27) Plasser, F.; Crespo-Otero, R.; Pederzoli, M.; Pittner, J.; Lischka, H.; Barbatti, M. Surface Hopping Dynamics with Correlated Single-Reference Methods: 9H-Adenine as a Case Study. *J. Chem. Theory Comput.* **2014**, *10*, 1395–1405.

(28) von Neumann, J.; Wigner, E. *The Collected Works of Eugene Paul Wigner*; Springer, 1993; pp 294–297.

(29) Teller, E. The Crossing of Potential Surfaces. *J. Phys. Chem.* **1937**, *41*, 109–116.

(30) Golub, G. H.; Van Loan, C. F. *Matrix computations*; JHU Press, 2012; Vol. 3.

(31) Anton, H.; Rorres, C. *Elementary Linear Algebra, Binder Ready Version: Applications Version*; John Wiley & Sons, 2013.

(32) Kjønstad, E. F.; Koch, H. Resolving the Notorious Case of Conical Intersections for Coupled Cluster Dynamics. *J. Phys. Chem. Lett.* **2017**, *8*, 4801–4807.

(33) Robinson, J. B.; Knowles, P. J. Approximate variational coupled cluster theory. *J. Chem. Phys.* **2011**, *135*, 044113.

(34) Kats, D.; Usvyat, D.; Schütz, M. Second-order variational coupled-cluster linear-response method: A Hermitian time-dependent theory. *Phys. Rev. A* **2011**, *83*, 062503.

(35) Wälz, G.; Kats, D.; Usvyat, D.; Korona, T.; Schütz, M. Application of Hermitian time-dependent coupled-cluster response Ansätze of second order to excitation energies and frequency-dependent dipole polarizabilities. *Phys. Rev. A* **2012**, *86*, 052519.

(36) Liu, J.; Asthana, A.; Cheng, L.; Mukherjee, D. Unitary coupled-cluster based self-consistent polarization propagator theory: A third-order formulation and pilot applications. *J. Chem. Phys.* **2018**, *148*, 244110.

(37) Hald, K.; Hättig, C.; Jørgensen, P. Triplet excitation energies in the coupled cluster singles and doubles model using an explicit triplet spin coupled excitation space. *J. Chem. Phys.* **2000**, *113*, 7765–7772.

(38) Larsen, H.; Hald, K.; Olsen, J.; Jørgensen, P. Triplet excitation energies in full configuration interaction and coupled-cluster theory. *J. Chem. Phys.* **2001**, *115*, 3015–3020.

(39) Helgaker, T.; Jorgensen, P.; Olsen, J. *Molecular electronic-structure theory*; John Wiley & Sons, 2014.

(40) Koch, H.; Jensen, H. J. A.; Jørgensen, P.; Helgaker, T.; Scuseria, G. E.; Schaefer, H. F. Coupled cluster energy derivatives. Analytic Hessian for the closed-shell coupled cluster singles and doubles wave function: Theory and applications. *J. Chem. Phys.* **1990**, *92*, 4924–4940.

(41) Koch, H.; Kobayashi, R.; Sanchez de Merás, A.; Jørgensen, P. Calculation of size-intensive transition moments from the coupled cluster singles and doubles linear response function. *J. Chem. Phys.* **1994**, *100*, 4393–4400.

(42) *The eT program will be described in a forthcoming publication*

(43) Folkestad, S. D.; Kjønstad, E. F.; Koch, H. An efficient algorithm for Cholesky decomposition of electron repulsion integrals. *J. Chem. Phys.* **2019**, *150*, 194112.

(44) Pulay, P. Convergence acceleration of iterative sequences. the case of scf iteration. *Chem. Phys. Letters* **1980**, *73*, 393 – 398.

(45) Hättig, C.; Weigend, F. CC2 excitation energy calculations on large molecules using the resolution of the identity approximation. *J. Chem. Phys.* **2000**, *113*, 5154–5161.

(46) Shao, Y.; Gan, Z.; Epifanovsky, E.; Gilbert, A. T.; Wormit, M.; Kussmann, J.; Lange, A. W.; Behn, A.; Deng, J.; Feng, X. Advances in molecular quantum chemistry contained in the Q-Chem 4 program package. *Mol. Phys.* **2015**, *113*, 184–215.

(47) Christiansen, O.; Koch, H.; Jørgensen, P.; Olsen, J. Excitation energies of H2O, N2 and C2 in full configuration interaction and coupled cluster theory. *Chem. Phys. Letters* **1996**, *256*, 185 – 194.

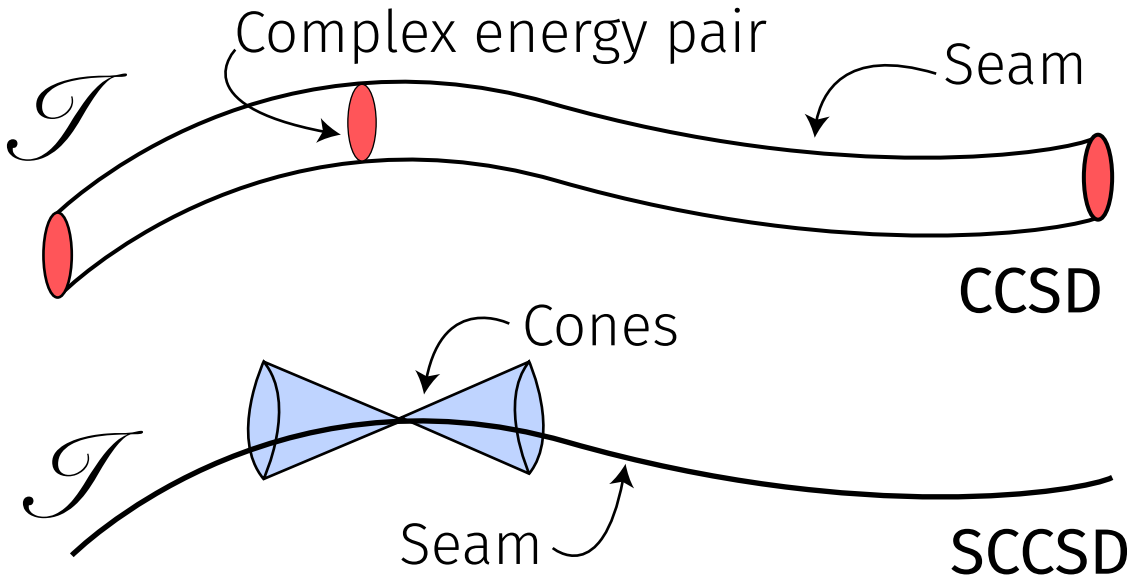
Complex energy pair
Seam
$\mathscr{T}$
CCSD
Cones
$\mathscr{T}$
Seam
SCCSD